This is an open access article published under a Creative Commons Attribution (CC-BY) License, which permits unrestricted use, distribution and reproduction in any medium, provided the author and source are cited.

ACS AUTHORCHOICE

ACS NANO

www.acsnano.org

ARTICLE

Citrate Coordination and Bridging of Gold Nanoparticles: The Role of Gold Adatoms in AuNP Aging

David-Benjamin Grys, Bart de Nijs, Andrew R. Salmon, Junyang Huang, Wenting Wang, Wei-Hsin Chen, Oren A. Scherman, and Jeremy J. Baumberg*

Cite This: *ACS Nano* 2020, 14, 8689–8696

Read Online

ACCESS | Metrics & More | Article Recommendations | Supporting Information

ABSTRACT: **Gold nanoparticles used in many types of nanostructure are mostly stabilized by citrate ligands. Fully understanding their dynamic surface chemistry is thus essential for applications, particularly since aging is frequently a problem. Using surface-enhanced Raman spectroscopy in conjunction with density functional theory calculations, we are able to determine Au−citrate coordination in liquid with minimal invasiveness. We show that citrate coordination is mostly bidentate and simply controlled by its protonation state. More complex binding motifs are caused by interfering chloride ions and gold adatoms. With increasing age of stored gold nanoparticle suspensions, gold adatoms are found to move atop the Au facets and bind to an additional terminal carboxylate of the citrate. Aged nanoparticles are fully refreshed by removing these adatoms, using etching and subsequent boiling of the gold nanoparticles.**

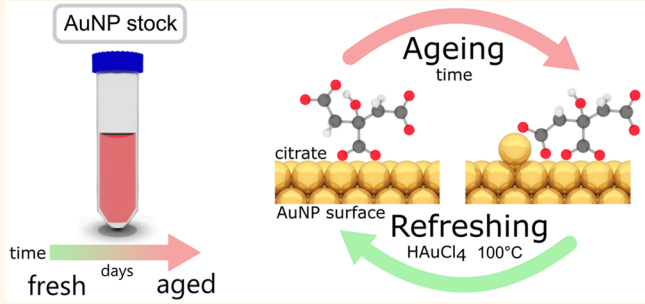

KEYWORDS: *nanogap, colloidal gold, gold atom movement, capping agent, ligand, SERS reproducibility, citrate binding*

Colloidal gold nanoparticles (AuNPs) form a fundamental building block in many applications across nanotechnology as well as underpinning natural science. Over recent decades, the synthesis of gold nanoparticles has been refined to yield diverse shapes, sizes, and coatings.[1−3] Such AuNPs are now utilized in immunoassays, drug-delivery systems, cancer therapy, catalysis, microscopy, nanorobots, chemical sensing, and many more applications.[4−7] Synthesis of the prototypical colloidal system for spherical gold nanoparticles is based on a simple reaction reducing auric acid with either sodium citrate or sodium borohydride. Sodium citrate is particularly interesting, as it is cheap and nontoxic and not only does it act as the reducing agent but its negatively charged carboxylates are also responsible for the charge stabilization of the AuNPs.

As applications for citrate-capped gold nanoparticles become ever more dependent on their precise surface chemistry, fully understanding the citrate coordination and most crucially time-dependent rearrangements (termed "aging") on the AuNP surfaces is now essential. Previous studies of citrate on metallic nanoparticles use various spectroscopic techniques including attenuated total reflectance infrared (ATR-IR),[8,9] Fourier transform infrared (FTIR),[10] X-ray photoelectron (XPS),[11] solid-state NMR,[12] and surface-enhanced Raman spectroscopy (SERS)[13,14] reporting a wide range of binding motifs (and contradicting each other). As demonstrated below, we believe that this wide disparity of results is caused by the high sensitivity of citrate binding to its chemical environment. In order to provide a more complete picture, it is crucial to take into account time dependence, pH, cations, and anions (specifically chloride) and also the reconstruction of the gold surface itself.

Here, we employ SERS, which is advantageous compared to previous techniques (ssNMR, ATR-IR, XPS), as it records the vibrational signatures of citrate anions directly in the liquid state and exclusively at the metal interfaces of colloidal gold nanoparticles. We investigate the effects of benign (Cucurbit[5]uril = CB[5]) and also more invasive (*e.g.*, NaCl) aggregating agents on citrate coordination. Our plasma-cleaned AuNP films that mimic colloidal Au clusters without

Received: April 10, 2020
Accepted: June 16, 2020
Published: June 16, 2020

© 2020 American Chemical Society

https://dx.doi.org/10.1021/acsnano.0c03050
ACS Nano 2020, 14, 8689–8696

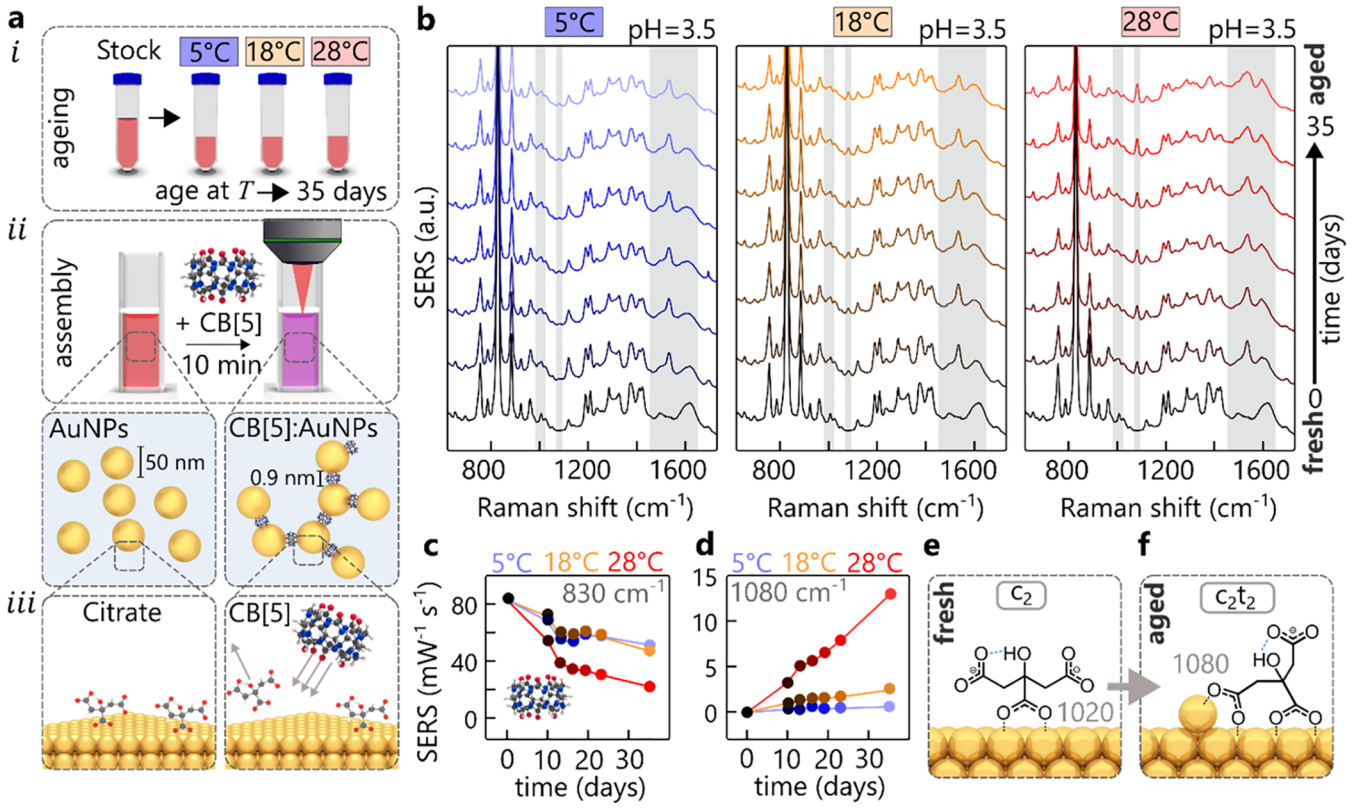

Figure 1. Aging of AuNPs. (a, *i*) Protocol of AuNP aging; (a, *ii*) protocol to form CB[5]:AuNP aggregates with precise nanogaps of 0.9 nm; (a, *iii*) depiction of CB[5] binding onto the AuNP surface displacing some of the citrate anions. (b) Aging experiment over 35 days showing SERS spectra of AuNP:CB[5] aggregates for AuNPs previously stored at 5, 18, and 28 °C. (c) Extracted CB[5] signature peak at 830 cm^{-1} (ring breathing mode). (d) Extracted citrate c_2t_2 peak at 1080 cm^{-1} for different temperatures in (b), normalized to the CB[5] signature peak. (e, f) Proposed citrate coordination in CB[5]:AuNP aggregates for fresh and aged AuNPs, showing influence of thermally activated Au adatoms.

the need for aggregating agents allow us to record SERS spectra in the absence of chloride and citrate decomposition products.

By this method, we provide strong evidence that the time- and temperature-dependent rearrangement of citrate anions (from μ_2 to μ_4, c_2 to c_2t_2, see Figure S6 for details on custom notation) on the AuNP surface (aging) is driven by migration of Au adatoms on the facet. As we show for CB[5], the increased binding affinity of citrate inhibits ligand exchange. Aged AuNPs can simply be "refreshed" by reconstructing the AuNP facets.

With additional parameters (age, pH, and ions), we find that it is possible to unify previous results on citrate coordination found in the literature: citrate coordinates in accordance with its protonation state preferring bidentate binding with both carboxylate oxygens over monodentate binding, which is only encountered in environments rich in chloride ions. For pH < 6.8 bidentate bridging of the central carboxylate (μ_2-1κO^1:2κO^3, c_2) is dominant, whereas only for pH > 6.8 are modes of the terminal carboxylates bound independently of the central carboxylate (*e.g.*, μ_4-1$\kappa O^{1'}$:2$\kappa O^{3'}$3$\kappa O^{1''}$:4$\kappa O^{3''}$, t_2t_2). In nanoparticle clusters with sufficiently small gap sizes, we also see citrate spanning across the nanogaps between neighboring nanoparticles. The presence or absence of the citrate spanning mode is a handy tool to estimate the gap size in AuNP nanoclusters.

RESULTS AND DISCUSSION

Observing Citrate Adatoms–AuNP Aging. Spherical gold nanoparticles synthesized using the standard Turkevich/Frens protocol serve as the basis of these aging investigations.[15,16] Stock AuNPs are synthesized to give average diameters of 50 ± 18 nm (Figure S1) at pH = 3.5 ± 0.1 and stored in three aliquots (50 mL polypropylene centrifuge tubes) at different temperatures, 5 ± 0.5, 18 ± 2, and 28 ± 5 °C (Figure 1a, *i*, for detailed AuNP characterization see Figure S1).

To probe the surface chemistry using SERS, the gold nanoparticles are aggregated into clusters with the help of the linker molecule cucurbit[5]uril (CB[5]), which acts as a precise molecular spacer (Figure 1a, *ii*, see Figure S2 for alternative salt aggregation).[17] A key advantage in employing CB[5] (instead of a salt) is the highly reproducible SERS spectra, which allow quantitative interpretation (such as calculating activation energies, Figure S3). The CB[5] molecules connect adjacent nanoparticles by displacing citrate (Figure 1a, *iii*) and binding to the gold surface *via* their carbonyl-rimmed portals.[18] Any subtle change of the nanoparticle surface chemistry is directly reflected in the SERS spectra.

Over the course of 35 d aging of the AuNPs, SERS spectra of freshly clustered CB[5]:AuNPs are taken after exactly 10 min of aggregation time, giving different spectra for the three aliquots stored at different temperatures (Figure 1b). Despite the excellent short-term reproducibility (<2%) of CB[5]:AuNP

https://dx.doi.org/10.1021/acsnano.0c03050
ACS Nano 2020, 14, 8689–8696

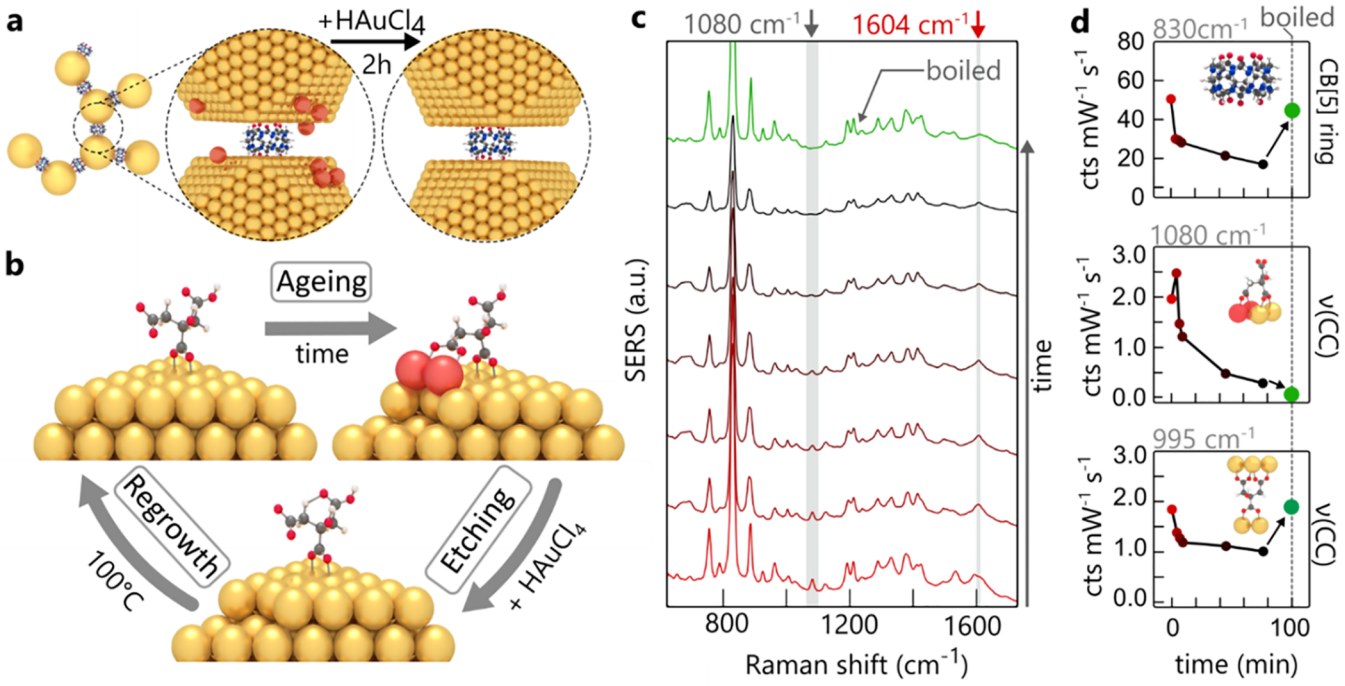

Figure 2. Refreshing gold nanoparticles. (a) Aging by adatoms (red) is reversed by adding $HAuCl_4$ to preformed CB[5]:AuNP aggregates assembled from aged AuNPs, followed by boiling for 5 min. (b) Model of aging/reversal process showing changing citrate coordination. (c) *In situ* time-dependent monitoring of SERS spectra during auric chloride etching (reactivation), with (d) SERS strengths from CB[5], 1080 cm^{-1} adatom, and 995 cm^{-1} gap-spanning citrate peaks.

aggregates (Figure S4), the overall CB[5] signal diminishes, as tracked by the CB[5] signature peak at 830 cm^{-1} (Figure 1c). The peak intensity drops by a half for T = 5 and 18 °C and even more for T = 28 °C to a quarter after 30 d. Concurrently, a range of peaks emerge, which are not related to the CB[5] molecule. These vibrations at 995, 1020, 1080, 1385, 1535, 1585, and 1604 cm^{-1} are ascribed to the presence of citrate anions on the gold surface inside the nanogaps (see DFT in Figures S5 and S6). The temporal evolution of these peaks suggests that citrate anions undergo temperature-dependent conformational changes (termed aging), which partially inhibits CB[5] binding.

Aggregates formed from AuNPs stored at T = 28 °C give rise to a strongly increasing 1080 cm^{-1} vibration with aging (Figure 1d). This comes from the ν(CC) stretch (see DFT in Figure S6) and appears at this position only if the central (c) and terminal (t) carboxylates are both bound (c_2t_2) to the same gold facet, forming a ring (Figure 1f). Here the subscript 2 indicates that a carboxylate has bidentate (μ_2-1κO^1:2κO^3) binding (Figure 1e), with monodentate binding (1κO^1) given by subscript 1 (see Figure S8 for kappa/mu convention naming scheme). This linear growth of the c_2t_2 binding is much slower at lower temperature, allowing extraction of its activation energy of ~1.1 ± 0.2 eV (see Figure S3). This strongly suggests that c_2t_2 binding can only occur upon reconstruction of the Au surface through adatoms, which possess similar calculated and measured activation energies on gold.[19,20] The emergence of the citrate-adatom peaks after aging shows that CB[5] molecules are no longer able to displace the citrate from the surface due to its greater (double) bidentate binding affinity. Eventually, this leads to loss of aggregation and changes in other AuNP chemistries. The time scales involved in this aging also match those for Au adatom formation and migration under ambient conditions, which explains for instance the need for refrigerated storage of SERS substrates (as for Klarite).[21] In order to rule out other effects, we investigate the role of monovalent cations and thermal decomposition of citrate byproducts. Repeating the aging experiment with nanoparticles synthesized with heavier K^+ cations instead of Na^+ yields exactly the same result (see Figure S7). The lack of any shifts in vibrational energies implies the role of cations can be neglected, as also suggested by computational studies.[22]

The SERS spectra of the citrate byproducts acetonedicarboxylate (ADC), acetoacetate (AA), and acetate do not match the peaks emerging in the aging experiments (see Figure S8). Such byproducts are formed during the AuNP reaction as citrate is consumed and also after the reaction through thermal decomposition. The activation energies for the thermal decomposition of ADC[23] and AA[24] are similar to the adatom activation energy. However, rapid decomposition through decarboxylation occurs within a few minutes to a maximum of a few days after AuNP synthesis (see see Tables S2 and S3 for rate calculations).[25] Gold nanoparticles synthesized directly from ADC do not resemble the aging peaks (see Figure S9). Swapping the supernatant between fresh and aged nanoparticles neither ages the fresh nor refreshes the aged particles. Finally, in a byproduct-free environment, the adatom-driven effect can also be reproduced (see section 4). It is thus implausible that the aging effects are caused by any citrate byproducts.

Citrate-Bound Adatoms: Reactivation *via* "Refacetting". Having shown strong evidence that Au adatoms control the chemical changes in ligand binding, we demonstrate how to reverse this aging by etching the AuNPs with a strong oxidizing agent such as auric chloride ($HAuCl_4$). This procedure removes weakly bound gold atoms from edges,

https://dx.doi.org/10.1021/acsnano.0c03050
ACS Nano 2020, 14, 8689−8696

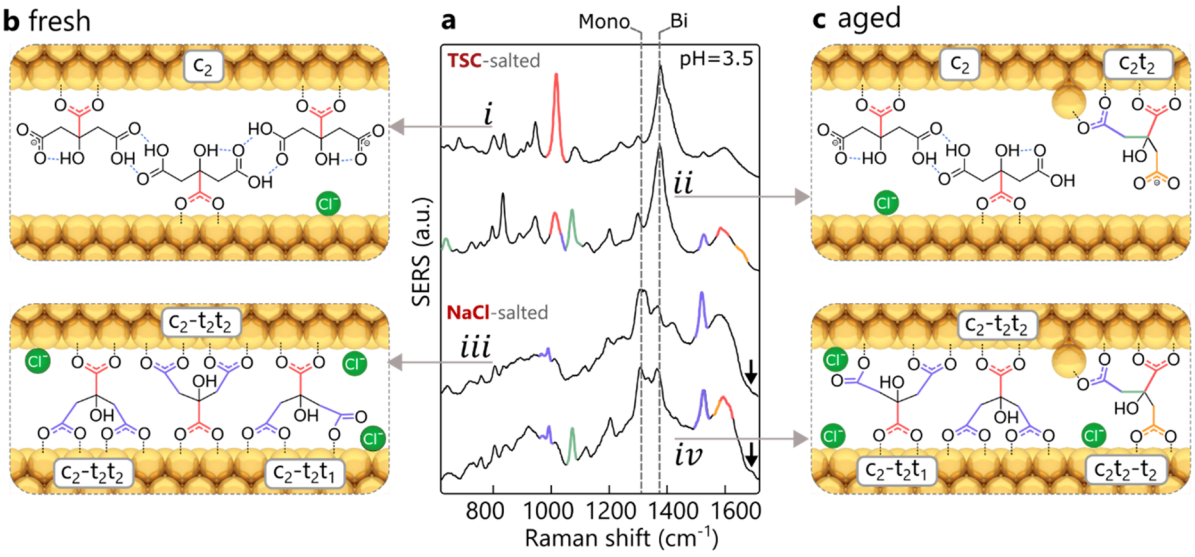

Figure 3. Citrate coordination in nanogaps. (a) SERS signals for both aggregation agents at pH = 3.5, using fresh and aged AuNPs. (b, c) Proposed models of citrate coordination inside nanogaps in AuNP aggregates for (b) freshly made or (c) aged nanoparticles, formed using excess trisodium citrate (top) or sodium chloride (bottom).

steps, and vertices[26,27] and therefore can attack gold adatoms coordinated to citrate anions (Figure 2a).

To monitor the etching process *in situ*, CB[5]-bound aggregates are formed over 10 min using aged gold nanoparticles. After aggregation, facet etching is initiated through addition of chloroauric acid to a final concentration of 125 μM. Since the acid is added to the AuNPs at room temperature, the presence of citrate does not induce nucleation or significant growth (see Figure S10), as is the case during NP synthesis. The *in situ* SERS spectra (Figure 2b) resolve citrate peaks showing rapid adatom removal through the disappearance of the 1080 cm^{-1} ν(CC) bidentate binding (Figure 2c). Detachment of the terminal carboxylates from adjacent AuNPs is also seen as the decay of citrate vibrations ν(CC) = 995 cm^{-1}, ν_a(COO) = 1535 cm^{-1}, and ν_a(COO) = 1585 cm^{-1}. The persisting ν_a(COO) = 1604 cm^{-1} vibration (Figure 2c, red arrow) shows that the central carboxylate remains bound (c_2).

Subsequent boiling in the presence of citrate anneals and reconstructs the etched facets, restoring the CB[5] SERS peak. The unbound terminal carboxylates again bind to the surface of the adjacent AuNP, giving terminal-spanning bound citrate but without evidence of any adatoms. The restored AuNP aggregates now behave with the same SERS sensing capability as previously observed. The control measurement, boiling aged AuNPs without adding $HAuCl_4$, leads to an increase of citrate adatom signals (see Figure S11).

Citrate Coordination in the Nanogap. From this understanding of aging as adatom-induced reconfiguration of citrate anions on gold facets, the general configuration of citrate ions inside nanogaps formed between adjacent nanoparticles can be investigated, for both fresh and aged nanoparticles.

To determine more carefully the citrate configurations inside smaller nanogaps, aggregates are instead formed by salting (reducing the screening length) using either concentrated sodium chloride (NaCl) or trisodium citrate (TSC) buffer solution with pH matching that of the nanoparticle suspension. For freshly made AuNPs aggregated with TSC, the SERS spectra (Figure 3a, *i*) reveal coordination only *via* the central carboxylate (c_2, red, bonds in Figure 3b). With full protonation of the non-surface-bound terminal carboxylates at pH = 3.5, neighboring citrate anions should form carboxylic acid dimers (seen in characteristic dimer vibrations at 1700−1715 cm^{-1}, see Figure S4), which are only weakly Raman active.[28]

Forming fresh AuNP aggregates instead with excess NaCl generates a different spectrum (Figure 3a, *iii*) in which the dominant citrate mode changes from c_2 to the gap-spanning c_2−t_2t_2 (995 cm^{-1}) (blue, bonds in Figure 3b). Here the dash (−) separates groups bound to different nanoparticle surfaces. In addition to the centrally bound carboxylate, the two terminal carboxylates also coordinate with the neighboring nanoparticle while spanning the nanogap (nanogap size estimate is 0.8 to 1.0 nm, see Figure S12). For this to occur, the citrate surface coverage needs to be low enough to allow access to the Au surface. For TSC-salted aggregates, addition of excess citrate instantaneously increases the surface coverage so that spanning cannot happen due to steric crowding, in contrast to NaCl aggregation. In addition to citrate rearrangement with NaCl, a distinct shift from bidentate to monodentate coordination is observed *via* the increasing C−O−Au stretch[29] at ∼1300 cm^{-1} (dashed vertical line) together with the decreasing 1385 cm^{-1} symmetric COO^-−Au stretch, as well as the emerging 1680 cm^{-1} C═O stretch of the unbound oxygen (black arrow). We speculate that addition of chloride anions near the gold surface (as surface chlorides) prevents citrate from bidentate binding.[30−32] Low-wavenumber vibrations ascribed to Au−Cl bonds indicate the presence of adsorbed chloride on the Au surface (see Figure S13).[33,34] Further control measurements using salts containing mono- or divalent anions with and without chloride ions ($MgCl_2$, $CaCl_2$, Na acetate, Mg citrate) confirm this hypothesis (see Figure S14).

Using aged nanoparticles with TSC (Figure 3a, *ii*), the characteristic ν(CC) vibration at 1080 cm^{-1} (marked in green, with bond in Figure 3c) clearly shows the adatom-induced c_2t_2 mode. The shoulder around 1630 cm^{-1} (orange, *ii*) for deprotonated carboxylates likely stems from the dangling terminal carboxylate of the c_2t_2 mode. Evidence is again seen for intermolecular hydrogen bonding *via* the carboxylic dimer formation (1700−1710 cm^{-1}) between c_2 citrates. Using

https://dx.doi.org/10.1021/acsnano.0c03050
ACS Nano 2020, 14, 8689−8696

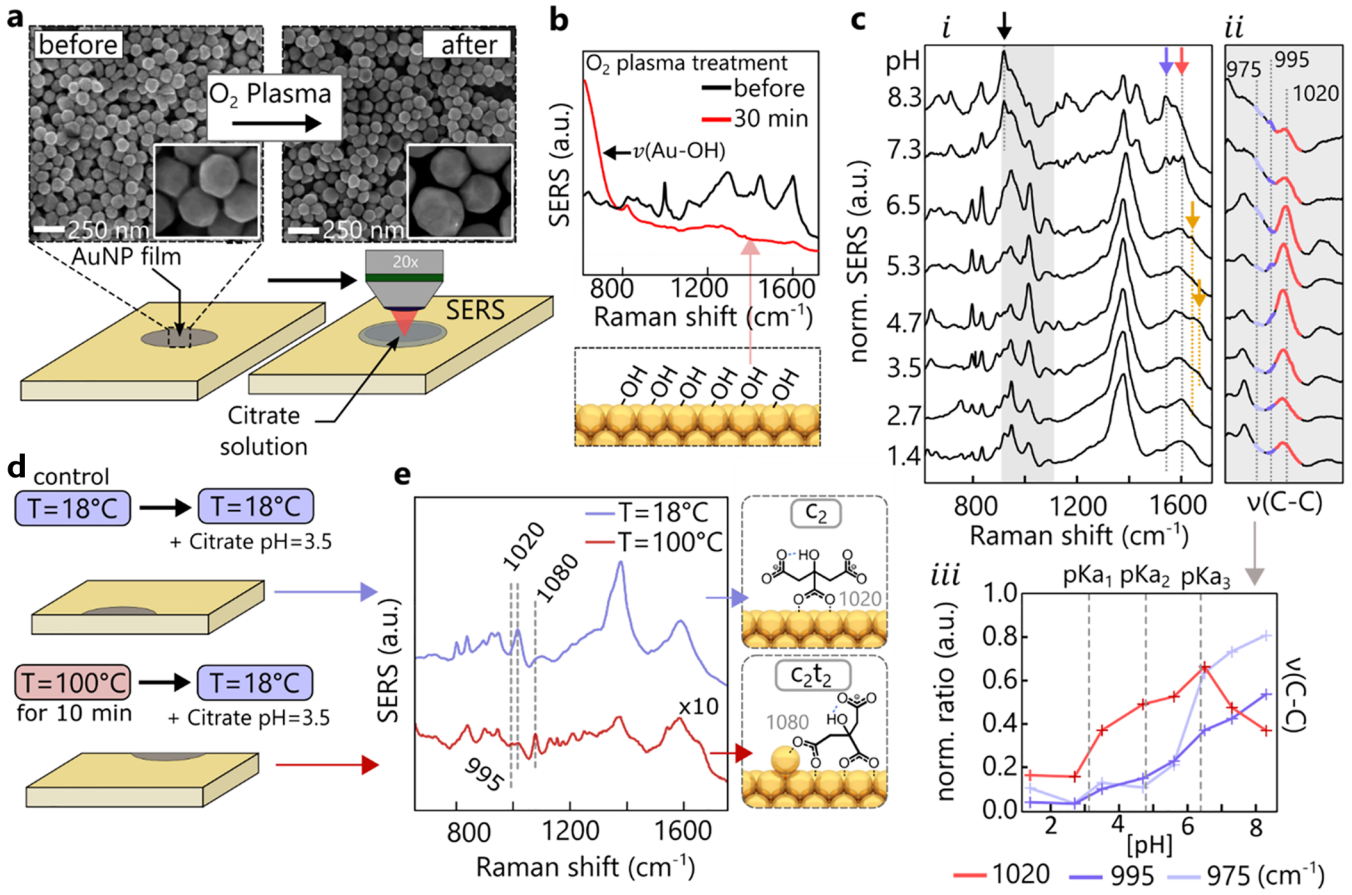

Figure 4. Organic-stripped AuNP films. (a) SEM images of AuNP films before and after O_2 plasma treatment with insets showing close-ups. (b) SERS spectra before and after O_2 plasma treatment, evidencing ligand removal and OH layer (from ambient moisture). (c) (*i*) SERS spectra normalized to symmetric carboxylate stretch at ~1380 cm^{-1} from treated AuNP films with added citrate *vs* pH, together with (*ii*) details of ν(CC) peak and (*iii*) peak ratios. (d) Experimental protocol of accelerated aging, showing heating of AuNP films directly after O_2 plasma cleaning leads to formation of adatoms, (e) seen in resulting SERS spectra. Heated films resemble adatom response of aged colloidal AuNPs.

NaCl-salted aged AuNP aggregates (Figure 3a, *iv*) gives very similar SERS spectra to the fresh AuNPs, apart from the adatom-induced c_2t_2 mode (green). An additional asymmetric carboxylate−Au stretch at 1585 cm^{-1} suggests that the adatom-coordinated citrate can also span the nanogap (orange, *iv*). This is supported by the disappearance of the shoulder at ~1630 cm^{-1} related to strain. Furthermore, loss of the 1020 cm^{-1} peak suggests that both (c,t) carboxylates are now fully coordinated. Evidence for monodentate binding from peaks at 1300 and 1680 cm^{-1} again suggests chloride ions interfere with bidentate binding.

Results for fresh and aged AuNPs buffered at higher pH values (most commercial NPs are stabilized close to pH = 7) suggest that more citrate coordination modes are present (Figure S2 and Table S1).

Citrate Coordination in AuNP Films. Salting of gold nanoparticles is thus invasive since it clearly changes how citrate is coordinated to the gold nanoparticle surface. To determine the intrinsic citrate signals, an alternative SERS substrate is employed consisting of 1−3 layers of close-packed nanoparticles. To remove all ligands (polymers, citrate, and all decomposition products) from the commercially synthesized nanoparticles employed, these substrates are O_2 plasma cleaned for 30 min. From the SEM images (Figure 4a, close-up in insets and Figure S15) it is evident that the AuNP shape remains intact and no bridges between particles are formed after treatment.[35] Comparing SERS measurements before and after the plasma treatment (Figure 4b) shows all organic compounds are removed from the films (red line), with only a layer of hydroxyl groups left on the surface (giving the low ν(Au−OH) = 590 cm^{-1} peak).

After immersing the treated films for 24 h in TSC solution, SERS spectra are taken with a droplet of the TSC solution left on the surface to maintain a similar environment to that for the suspended aggregates. To investigate the pH-dependence of citrate binding, a pH series between 1.4 and 8.3 is prepared by immersing the films in mixtures of TSC and citric acid. The SERS spectra (Figure 4c, *i*) resemble those of the TSC-salted colloidal aggregates (as compared to Figure S4). The absence of 1300 and 1680 cm^{-1} peaks implies that coordination is purely through bidentate bridging. Again, the addition of chloride ions to the AuNP films instantaneously generates some monodentate coordination as for colloidal aggregates salted with NaCl (see Figure S16).

Tracking the CC stretches (Figure 4c, *ii*, *iii*) shows that the citrate coordination modes reflect the protonation states of citrate set by its three pK_a values at 3.13 (central carboxylate) and 4.76 and 6.39 (terminal carboxylates).[36] Below pH = 6.5 citrate binding is again dominated by the 1020 cm^{-1} vibration and therefore the c_2 mode (Figure 4c, *ii*, *iii*, red). There is

https://dx.doi.org/10.1021/acsnano.0c03050
ACS Nano 2020, 14, 8689−8696

Table 1. Summary of Experiments Carried Out to Support the Hypothesis of Citrate Reconfiguration Driven by the Formation of Gold Adatoms

Experiment	Parameter	Conditions	Key results	Figure
AuNP:CB[5] aging	time	0 to 35 days aging	adatom signals emerge over time	1
AuNP:CB[5] aging	cations time	trisodium (Na^+) *vs* tripotassium (K^+) citrate AuNPs	same adatom signals over time, no influence of cations	S7
AuNPs salted (NaCl, TSC) aging	time pH	5 mM, citrate-buffered pH = 3.8, 5.5, 6.8	adatom signals observed, less intense for higher pH	S2
SERS of decomposition products		AuNP film *vs* suspension	peak positions not related to citrate adatoms	S8
acetone-dicarboxylate AuNPs		fresh *vs* aged	peak positions not related to citrate adatoms	S9
AuNP boiling with $HAuCl_4$		pH = 3.5 (before addition of $HAuCl_4$)	aging peaks removed	2
AuNP boiling without $HAuCl_4$		pH = 3.5	aging peaks intensify	S11
AuNP film accelerated aging		film heated to T = 100 °C, then exposed to TSC solution	adatom peaks same as in solution	4(e,f)
AuNP film aging	time	0 to 87 days	adatom peaks not observed, but citrate bridges AuNPs	S17

evidence of dangling carboxylates for 3.5 < pH < 5.3 (Figure 4c, *i*, orange arrow), but the absence of a strong 1080 cm^{-1} vibration suggest that the adatom-driven mode c_2t_2 is not present. Instead with a further increase of pH, spanning of the nanogap with the modes c_2−t_2 and c_2−t_2t_2 occurs, as seen by the emerging vibrations at 975 cm^{-1} (light blue) and 995 cm^{-1} (dark blue). Above pH = 6.5 (where most commercial NPs are stabilized) a decrease of 1020 cm^{-1} and steep increase of 975 cm^{-1} vibrations are observed. Along with the loss of the central (red arrow) and gain of the terminal (blue arrow) asymmetric COO^-−Au stretches, additional citrate binding with only the terminal carboxylates is found (Figure 4c, *i*). The strong $\nu(CCOO^-)$ mode (black arrow) at 925 cm^{-1} related to the unbound central carboxylate is only present for t_2t_2 coordination.

Aging in AuNP Films. There are two separate pathways for the aging of AuNP films and suspensions. For aged AuNP films with their close-packed AuNPs (pH = 3.5, 18 °C), the citrate anions preferentially span the gap (c_2-t_2t_2) with both terminal carboxylates (Figure S17). This is different from aging of suspended individual AuNPs, where spanning cannot occur. Instead, migrating adatoms attract one of the terminal carboxylates to form the c_2t_2 mode. After aggregation, the c_2t_2 mode can then transition to c_2t_2−t_2 inside the nanogaps depending on the gap size.

In order to observe the c_2t_2 mode in AuNP films, adatoms have to be generated before the films are immersed in TSC solution. This is achieved by heating a plasma-cleaned film to ∼100 °C for 10 min (Figure 4e). After cooling to room temperature, control and heated films are immersed in the same TSC solution for 24 h. The SERS spectra from the heated AuNP films (Figure 4e) resemble those of aged colloidal aggregates, showing the c_2t_2 modes together with c_2−t_2t_2. The control sample exhibits only the usual c_2 mode as expected for pH = 3.5. This shows that a detailed understanding of the citrate-binding modalities and the SERS peaks produced allows a full reconstruction and control of the citrate ligands on gold.

Overview of Adatom Experiments. A summary of experiments supporting the adatom-driven reconfiguration of citrate anions on the AuNP surface is shown in Table 1. It contains the name of each experiment, the parameters that have been controlled, the experimental conditions, and its key results. To make it easier for the reader to find the data, we have added references to the corresponding figures in the main text and also the Supporting Information.

CONCLUSION

Our analysis of the SERS of colloidal gold in liquid provides a nuanced account of the complexity of citrate binding to Au, which has previously led to a wide variety of interpretations. By analyzing multiple parameters such as pH, time-dependence (aging), and the influence of the chemical environment (chloride), we are able to provide a complete picture of citrate coordination.

We show that the dominant coordination mode of citrate (pH < 6.8) is the bidentate bridging of the central carboxylate (c_2). For even higher pH values (>6.8), unbound central carboxylates can be seen. We prove that surface-bound citrate anions almost exclusively prefer bidentate over monodentate binding. Only in a chloride-rich environment is monodentate binding present. For citrate trapped inside sub-nanometer gaps, citrate molecules can be observed to span across the nanogap while coordinating all three carboxylates in either the c_2−t_2t_2 or c_2t_2−t_2 modes for fresh or aged nanoparticles, respectively.

With increasing age of stored gold nanoparticle suspensions, gold adatoms move atop the Au facets and bind to one of the terminal carboxylates, yielding the double bidentate bridging mode (c_2t_2). These are rather stable, making citrate difficult to remove or undergo surface diffusion. We find that the adatom signals are independent of monovalent cations (K^+ *vs* Na^+) and also of citrate decomposition products present in solution. To what extent the adatom−citrate complex and its formation kinetics depend on the type of surface facets is still an open question.

Aged nanoparticles can be fully refreshed by removing these adatoms, using etching, and subsequent boiling of the gold nanoparticles. Our demonstration that Au adatoms play a crucial role gives much better control of their utilization for sensing and other nanoassembly-based technologies. This is crucial for widespread adoption in new generations of functional materials and devices.

EXPERIMENTAL METHODS

AuNP Synthesis. Sodium citrate tribasic dihydrate, potassium citrate tribasic monohydrate, lithium citrate tribasic tetrahydrate, and tetrachloroauric(III) acid trihydrate of analytical grade were purchased from Merck/Sigma-Aldrich. To yield particles with an average diameter of ∼50 nm, a gold/citrate ratio of 1.33 is employed.

https://dx.doi.org/10.1021/acsnano.0c03050
ACS Nano 2020, 14, 8689−8696

A 2.28 mL amount of a 152 mM solution of citrate was added to 150 mL of a 0.38 mM chloroauric acid solution under reflux with vigorous stirring. Reflux was continued for a further 15 min after the citrate addition. The resulting wine-red suspension was allowed to cool to room temperature for 1 h.

AuNP Films. For the AuNP films, 80 nm diameter commercial gold nanoparticles from BBI Solutions were purchased directly from the manufacturer. A total volume of 1 mL with equal parts of chloroform and the AuNP suspension were added to an Eppendorf tube, forming a two-phase system. After the addition of 150 μL of 1 M NaCl, the Eppendorf tube was shaken for 10 seconds. In this step, the majority of the nanoparticles are pushed to the interface of the aqueous phase. The supernatant is replaced three times with DI water to wash the particles. The supernatant/DI water was then almost fully removed, yielding a small droplet of concentrated AuNPs at the chloroform/water interface. Subsequently, the droplet was transferred onto an evaporated gold silicon wafer substrate. After the water fully evaporated, the films were washed with DI water and then oxygen plasma cleaned for 30 min using a Diener electronic GmbH & Co. KG plasma etcher. Lastly, the films were immersed in the analyte of interest for 24 h.

SERS/Raman Measurements. All Raman and SERS measurements used a Renishaw inVia Raman instrument. The excitation source is a 785 nm infrared laser with 147 mW of laser power available at the objective. For solution measurements, the focal plane of the 5× objective was always set to slightly below the air/liquid interface by maximizing the counts through a *z*-axis scan. Each solution spectrum was taken with full laser power 10 seconds integration time (if not otherwise stated) and integrated over three acquisitions. For the measurements of AuNP films, a 20× objective was focused using an imaging camera. The integration time was set to 10 seconds and three acquisitions were taken, with the laser power limited to 0.5% of full power. Liquid measurements were performed using polypropylene 96-well plates with 340 μL capacity per well.

AuNP Aggregate Preparation. For the formation of CB[5]:AuNP aggregates, 6.3 μL of a 125 μM solution of CB[5], synthesized and separated according to the protocol mentioned by Barrow *et al.*,[37] was added to 333 μL of the homemade nanoparticles. Exactly 10 min was allowed for nanoclusters to form before taking SERS spectra. Salted nanoparticles were prepared by using 30 μL of 0.5 M NaCl solution or 1 M citrate solution. For the pH experiments, the pH of the citrate solution was adjusted by mixing 1 M trisodium citrate and 1 M citric acid.

DFT Calculations. Geometry optimization and frequency calculation were performed using the hybrid functional PBE0 (PBE1PBE) with the 6-311++G(d,p) basis set and the Los Alamos ECP double-ζ basis set for Au atoms and clusters.[38] Solvent effects were considered using the polarizable continuum model (PCM) solvation model. For all calculations the Gaussian 09 *ab initio* software suite was employed.[39] The Raman intensities were corrected for the uniform polarizability in the plasmonic gaps. This is achieved by extracting the polarizability tensors from the Gaussian output file and recalculating the intensities.[40]

ASSOCIATED CONTENT

Supporting Information

The Supporting Information is available free of charge at https://pubs.acs.org/doi/10.1021/acsnano.0c03050.

Additional Figures S1−S17 and Tables S1−S3 (PDF)

AUTHOR INFORMATION

Corresponding Author

Jeremy J. Baumberg − *NanoPhotonics Centre, Cavendish Laboratory, Department of Physics, JJ Thompson Avenue, University of Cambridge, Cambridge CB3 0HE, U.K.;* orcid.org/0000-0002-9606-9488; Email: jjb12@cam.ac.uk

Authors

David-Benjamin Grys − *NanoPhotonics Centre, Cavendish Laboratory, Department of Physics, JJ Thompson Avenue, University of Cambridge, Cambridge CB3 0HE, U.K.;* orcid.org/0000-0002-4038-6388

Bart de Nijs − *NanoPhotonics Centre, Cavendish Laboratory, Department of Physics, JJ Thompson Avenue, University of Cambridge, Cambridge CB3 0HE, U.K.*

Andrew R. Salmon − *NanoPhotonics Centre, Cavendish Laboratory, Department of Physics, JJ Thompson Avenue, University of Cambridge, Cambridge CB3 0HE, U.K.;* orcid.org/0000-0001-6267-5896

Junyang Huang − *NanoPhotonics Centre, Cavendish Laboratory, Department of Physics, JJ Thompson Avenue, University of Cambridge, Cambridge CB3 0HE, U.K.*

Wenting Wang − *NanoPhotonics Centre, Cavendish Laboratory, Department of Physics, JJ Thompson Avenue, University of Cambridge, Cambridge CB3 0HE, U.K.*

Wei-Hsin Chen − *NanoPhotonics Centre, Cavendish Laboratory, Department of Physics, JJ Thompson Avenue, University of Cambridge, Cambridge CB3 0HE, U.K.*

Oren A. Scherman − *Melville Laboratory for Polymer Synthesis, Department of Chemistry, University of Cambridge, Cambridge CB2 1EW, U.K.;* orcid.org/0000-0001-8032-7166

Complete contact information is available at: https://pubs.acs.org/10.1021/acsnano.0c03050

Notes

The authors declare no competing financial interest.
Source data can be found at 10.17863/CAM.53701.

ACKNOWLEDGMENTS

We acknowledge financial support from EPSRC Grants (EP/L027151/1, EP/R020965/1, EP/P029426/1, and EP/L015889/1). B.d.N. acknowledges support from the Leverhulme Trust, the Isaac Newton Trust, and support from the Winton Foundation for the Physics of Sustainability. We greatly appreciate useful discussions with C. Jones (BBI).

REFERENCES

(1) Kumar, P. S.; Pastoriza-Santos, I.; Rodriguez-Gonzalez, B.; de Abajo, F. J. G.; Liz-Marzan, L. M. High-Yield Synthesis and Optical Response of Gold Nanostars. *Nanotechnology* **2008**, *19*, 1−6.

(2) Murphy, C. J.; Gole, A. M.; Hunyadi, S. E.; Stone, J. W.; Sisco, P. N.; Alkilany, A.; Kinard, B. E.; Hankins, P. Chemical Sensing and Imaging with Metallic Nanorods. *Chem. Commun.* **2008**, No. 5, 544−557.

(3) Mine, E.; Yamada, A.; Kobayashi, Y.; Konno, M.; Liz-Marzán, L. M. Direct Coating of Gold Nanoparticles with Silica by a Seeded Polymerization Technique. *J. Colloid Interface Sci.* **2003**, *264*, 385−390.

(4) Liu, X.; Dai, Q.; Austin, L.; Coutts, J.; Knowles, G.; Zou, J.; Chen, H. A One-Step Homogeneous Immunoassay for Cancer Biomarker Detection Using Gold Nanoparticle Probes Coupled with Dynamic Light Scattering. *J. Am. Chem. Soc.* **2008**, *130*, 2780−2782.

(5) Douglas, S. M.; Bachelet, I.; Church, M. G. A Logic-Gated Nanorobot for Targeted Transport of Molecular Payloads. *Science* **2012**, *335*, 831−834.

(6) Turner, M.; Golovko, V. B.; Vaughan, O. P. H.; Abdulkin, P.; Berenguer-Murcia, A.; Tikhov, M. S.; Johnson, B. F. G.; Lambert, R. M. Selective Oxidation with Dioxygen by Gold Nanoparticle Catalysts Derived from 55-Atom Clusters. *Nature* **2008**, *454*, 981−984.

(7) Saha, K.; Agasti, S. S.; Kim, C.; Li, X.; Rotello, V. M. Gold Nanoparticles in Chemical and Biological Sensing. *Chem. Rev.* **2012**, *112*, 2739−2779.

(8) Park, J. W.; Shumaker-Parry, J. S. Structural Study of Citrate Layers on Gold Nanoparticles: Role of Intermolecular Interactions in Stabilizing Nanoparticles. *J. Am. Chem. Soc.* **2014**, *136*, 1907−1921.
(9) Park, J. W. Negative-Imaging of Citrate Layers on Gold Nanoparticles by Ligand-Templated Metal Deposition: Revealing Surface Heterogeneity. *Part. Part. Syst. Charact.* **2019**, *36*, 1−9.
(10) Wulandari, P.; Nagahiro, T.; Michioka, K.; Tamada, K.; Ishibashi, K.; Kimura, Y.; Niwano, M. Coordination of Carboxylate on Metal Nanoparticles Characterized by Fourier Transform Infrared Spectroscopy. *Chem. Lett.* **2008**, *37*, 888−889.
(11) Mikhlin, Y. L.; Vorobyev, S. A.; Saikova, S. V.; Vishnyakova, E. A.; Romanchenko, A. S.; Zharkov, S. M.; Larichev, Y. V. Applied Surface Science on the Nature of Citrate-Derived Surface Species on Ag Nanoparticles: Insights from X-Ray Photoelectron Spectroscopy. *Appl. Surf. Sci.* **2018**, *427*, 687−694.
(12) Al-Johani, H.; Abou-Hamad, E.; Jedidi, A.; Widdifield, C. M.; Viger-Gravel, J.; Sangaru, S. S.; Gajan, D.; Anjum, D. H.; Ould-Chikh, S.; Hedhili, M. N.; Gurinov, A.; Kelly, M. J.; Eter, M. El; Cavallo, L.; Emsley, L.; Basset, J. M. The Structure and Binding Mode of Citrate in the Stabilization of Gold Nanoparticles. *Nat. Chem.* **2017**, *9*, 890−895.
(13) Munro, C. H.; Smith, W. E.; Garner, M.; Clarkson, J.; White, P. C. Characterization of the Surface of a Citrate-Reduced Colloid Optimized for Use as a Substrate for Surface-Enhanced Resonance Raman-Scattering. *Langmuir* **1995**, *11*, 3712−3720.
(14) Mabuchi, M.; Takenaka, T.; Fijiyoshi, Y.; Uyeda, N. Surface Enhanced Raman Scattering of Citrate Ions Adsorbed on Gold Sol Particles. *Surf. Sci.* **1982**, *119*, 150−158.
(15) Turkevich, J.; Stevenson, P. C.; Hillier, J. A Study of the Nucleation and Growth Processes in the Synthesis of Colloidal Gold. *Discuss. Faraday Soc.* **1951**, *11*, 55−75.
(16) Frens, G. Controlled Nucleation for the Regulation of the Particle Size in Monodisperse Gold Suspensions. *Nature, Phys. Sci.* **1973**, *241*, 20−22.
(17) Kasera, S.; Hermann, L. O.; Del Barrio, J.; Baumberg, J. J.; Scherman, O. A. Quantitative Multiplexing with Nano-Self-Assemblies in SERS. *Sci. Rep.* **2015**, *4*, 1−6.
(18) Mahajan, S.; Lee, T.-C.; Biedermann, F.; Hugall, J. T.; Baumberg, J. J.; Scherman, O. A. Raman and SERS Spectroscopy of Cucurbit[n]Urils. *Phys. Chem. Chem. Phys.* **2010**, *12*, 10429−10433.
(19) Benz, F.; Schmidt, M. K.; Dreismann, A.; Chikkaraddy, R.; Zhang, Y.; Demetriadou, A.; Carnegie, C.; Ohadi, H.; Nijs, B. De; Esteban, R.; Aizpurua, J.; Baumberg, J. J. Single-Molecule Optomechanics in "Picocavities. *Science* **2016**, *354*, 726−730.
(20) Thompson, D.; Liao, J.; Nolan, M.; Quinn, A. J.; Nijhuis, C. A.; Dwyer, C. O.; Nirmalraj, P. N.; Scho, C.; Calame, M. Formation Mechanism of Metal-Molecule-Metal Junctions: Molecule-Assisted Migration on Metal Defects. *J. Phys. Chem. C* **2015**, *119*, 19438−19451.
(21) Hugall, J. T.; Baumberg, J. J.; Mahajan, S. Disentangling the Peak and Background Signals in Surface-Enhanced Raman Scattering. *J. Phys. Chem. C* **2012**, *116*, 6184−6190.
(22) Nara, M.; Torii, H.; Tasumi, M. Correlation between the Vibrational Frequencies of the Carboxylate Group and the Types of Its Coordination to a Metal Ion: An *Ab Initio* Molecular Orbital Study. *J. Phys. Chem.* **1996**, *3654*, 19812−19817.
(23) Larson, D. W.; Lister, M. W. Catalytic Decomposition of Acetonedicarboxylic Acid. *Can. J. Chem.* **1968**, *46*, 823−832.
(24) Hay, B. R. W.; Bond, M. A. Kinetics of the Decarboxylation of Acetoacetic Acid. *Aust. J. Chem.* **1967**, *20*, 1823−1828.
(25) Doyen, M.; Bartik, K.; Bruylants, G. Journal of Colloid and Interface Science UV - Vis and NMR Study of the Formation of Gold Nanoparticles by Citrate Reduction: Observation of Gold - Citrate Aggregates. *J. Colloid Interface Sci.* **2013**, *399*, 1−5.
(26) Lee, Y.; Schade, N. B.; Sun, L.; Fan, J. A.; Bae, D. R.; Mariscal, M. M.; Lee, G.; Capasso, F.; Sacanna, S.; Manoharan, V. N.; Yi, G. Ultrasmooth, Highly Spherical Monocrystalline Gold Particles for Precision Plasmonics. *ACS Nano* **2013**, *7*, 11064−11070.
(27) Li, C.; Shuford, K. L.; Chen, M.; Lee, E. J.; Cho, S. O. A Facile Polyol Route to Uniform Gold Octahedra with Tailorable Size and Their Optical Properties. *ACS Nano* **2008**, *2*, 1760−1769.
(28) Tanaka, N.; Kitano, H.; Ise, N. Raman Spectroscopic Study of Hydrogen Bonding in Aqueous Carboxylic Acid Solutions. 3. Polyacrylic Acid. *Macromolecules* **1991**, *24*, 3017−3019.
(29) Gao, X.; Davies, J. P.; Weaver, M. J. A Test of Surface Selection Rules for Surface-Enhanced Raman Scattering: The Orientation of Adsorbed Benzene and Monosubstituted Benzenes on Gold. *J. Phys. Chem.* **1990**, *94*, 6858−6864.
(30) Company, N. P.; Spencer, N. D.; Lambert, R. M. Chlorine Chemisorption and Surface Chloride Formation on Au(111). *Surf. Sci.* **1981**, *107*, 237−248.
(31) Park, J.; Shumaker-Parry, J. S. Strong Resistance of Citrate Anions on Metal Nanoparticles to Desorption under Thiol Functionalization. *ACS Nano* **2015**, *9*, 1665−1682.
(32) Zhao, L.; Jiang, D.; Cai, Y.; Ji, X.; Xie, R.; Yang, W. Nanoscale Tuning the Size of Gold Nanoparticles in the Citrate Reduction by Chloride Ions. *Nanoscale* **2012**, *4*, 5071−5076.
(33) Gao, P.; Weaver, M. J. Metal-Adsorbate Vibrational Frequencies as a Probe of Surface Bonding: Halides and Pseudohalides at Gold Electrodes. *J. Phys. Chem.* **1986**, *90*, 4057−4063.
(34) Murphy, P. J.; LaGrange, M. S. Raman Spectroscopy of Gold Chloro-Hydroxy Speciation in Fluids at Ambient Temperature and Pressure: A Re-Evaluation of the Effects of PH and Chloride Concentration. *Geochim. Cosmochim. Acta* **1998**, *62*, 3515−3526.
(35) Berman, D.; Krim, J. Impact of Oxygen and Argon Plasma Exposure on the Roughness of Gold Film Surfaces. *Thin Solid Films* **2012**, *520*, 6201−6206.
(36) Martin, R. B. A Complete Ionization Scheme for Citric Acid. *J. Phys. Chem.* **1961**, *1274*, 8−10.
(37) Barrow, S. J.; Kasera, S.; Rowland, M. J.; Del Barrio, J.; Scherman, O. A. Cucurbituril-Based Molecular Recognition. *Chem. Rev.* **2015**, *115*, 12320−12406.
(38) Hay, P. J.; Wadt, W. R. *Ab Initio* Effective Core Potentials for Molecular Calculations. Potentials for the Transition Metal Atoms Sc to Hg. *J. Chem. Phys.* **1985**, *82*, 270−283.
(39) Frisch, M. J.; Trucks, G. W.; Schlegel, H. B.; Scuseria, G. E.; Robb, M. A.; Cheeseman, J. R.; Scalmani, G.; Barone, V.; Petersson, G. A.; Nakatsuji, H.; Li, X.; Caricato, M.; Marenich, A. V.; Bloino, J.; Janesko, B. G.; Gomperts, R.; Mennucci, B.; Hratchian, H. P.; Ortiz, J. V.; Izmaylov, A. F.; et al. *Gaussian 09*, revision D.01; Gaussian, Inc.: Wallingford, CT, 2016.
(40) Le Rue, E.; Etchegoin, P. G. *Principles of Surface-Enhanced Raman Spectroscopy*, 1st ed.; Le Ru, E. C., Etchegoin, P. G., Eds.; Elsevier Ltd: Amsterdam, 2009; pp 474−479.

https://dx.doi.org/10.1021/acsnano.0c03050
ACS Nano 2020, 14, 8689−8696